Proceedings of the 1991 IEEE
International Conference on Robotics and Automation
Sacramento, California - April 1991

DESIGN OF COMPONENTS FOR PROGRAMMABLE PASSIVE IMPEDANCE

Kirsten F. Laurin-Kovitz
J. Edward Colgate
Steven D. R. Carnes

Department of Mechanical Engineering
Northwestern University
Evanston, IL 60208

ABSTRACT

Interactive tasks, such as parts assembly, require robots to perform compliant motion. Two common methods exist for producing compliance: active force feedback control and passive mechanical elements in the robot hardware. The former can be used in a variety of tasks but is subject to contact instability associated with the feedback loop time delay. The latter guarantees stability but has limited programmability. Proposed here is a form of impedance control which addresses the issue of stability as well as providing programmability of robots for interactive tasks. Passive mechanical elements, specifically springs and dampers, are incorporated into the drive of a robot. The impedance of the robot is programmable because the stiffness and damping coefficients of these mechanical elements are themselves programmable. The design of these elements and their use is outlined. Prototype springs and dampers have been fabricated and their performance in theory and in practice is discussed.

1. INTRODUCTION

It is generally recognized that, to perform tasks requiring energetic interaction with the environment, i.e., tasks such as parts assembly or tool use, robotic manipulators must exhibit some measure of *compliance* [18]. The subject of this paper is the *implementation* of compliance: an implementation of compliance control which is both robust and versatile has, to date, proven elusive. According to Mason [12], "There are two basic ways to produce compliant motion: a passive mechanical compliance built in to the manipulator or an active compliance implemented in the software control loop, also known as force control."

Passive mechanical compliance, in the form of the remote center of compliance (RCC) is the oldest, and possibly the most successful, implementation of compliance [14]. The RCC, however, provides the correct compliance for peg-in-hole insertion only, and therefore does not exhibit that hallmark of robotics: *programmability*. Programmability is more than a hallmark, however. It is necessary for the implementation of compliance control schemes for error-corrective assembly [15] and parts fixturing [16].

Implementing compliance via force control is an obvious route past this limitation, and is a topic that has received tremendous study in the past ten to fifteen years. Whitney provides an excellent review [18]. Standard implementations of force control, however, are subject to *contact instability*, which severely restricts the speed with which interactive tasks can be executed. Contact instability has been studied by a number of researchers [6], [11], [2]; the analysis in [3] shows that contact instability is, for practical purposes, an unavoidable consequence of closing a force feedback loop around a non-backdriveable robot.

In part because of this difficulty with non-backdriveable robots, a number of investigators have studied force control and impedance control implementations on direct drive (backdriveable) robots [1], [8]. While this approach shows some promise for realizing both programmability and robustness to contact, it also reflects certain undesirable characteristics of direct drive robots. For instance, motor and amplifier nonlinearities are particularly severe in direct drive designs, the number of degrees of freedom is typically limited because the massive motors must be base-mounted, and energy inefficiency is a problem; even holding a weight against gravity requires a constant energy expenditure.

In this paper, an approach to compliance control which is intended to help realize the goal of robust and programmable compliance is presented. This approach is *Programmable Passive Impedance* (PPI). It is proposed that the impedance of a robot may be controlled by incorporating programmable mechanical elements into the robot's drive system. A conceptual design of a one-link manipulator is shown in Figure 1. A non-backdriveable actuator, emphasized by the worm gear, drives the link through a transmission with programmable stiffness and viscous damping coefficients.

These *PPI components* combine the features of passivity for stability/robustness and programmability for versatility. Actual mechanical elements, in this case springs and dampers, are added to the robot hardware to provide open loop control during interactive tasks. This allows direct response to endpoint forces, torques, etc. and eliminates contact instability. By designing mechanical elements whose characteristics (stiffness or damping coefficient) can be changed, the impedance of the system can be altered to fit a variety of tasks or to react to sensed forces, positions and velocities. Feedback can still be used to supplement the mechanical elements, increasing dynamic range and improving linearity.

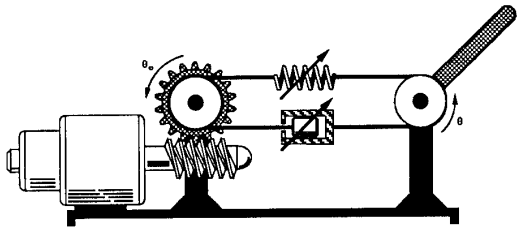

Figure 1: Conceptual design of a one-link manipulator with PPI. The transmission has programmable stiffness and viscous damping coefficients.

Recently, a number of researchers have developed robot components with programmability. Goswami [7] describes the use of hydraulic cylinders to provide a passive wrist with programmable accommodation. Cutkosky [5] extends the number of compliance centers available from a passive wrist by adding pressure-controlled, fluid-filled bladders. Mills [13] uses hybrid actuators consisting of a d.c. servo motor paired with a pneumatic bladder actuator to vary manipulator stiffness. Immega [10] suggests that pneumatic bladders may be used to provide both actuation and compliance control.

This paper introduces two components for PPI, a tuneable damper and a tuneable spring. These components have been designed for eventual use in a multiple degree of freedom manipulator; therefore, requirements of small size and weight, and large dynamic range have driven the designs. Linear designs which simplify the programming of a complex system are also desirable. In the next section, the design of the tuneable damper is outlined. Section 3 describes the tuneable spring design, and section 4 contains a discussion of the incorporation of the spring and damper into a single degree of freedom manipulator.

2. THE BINARY DAMPER

A survey of commercially available dampers clearly indicates that hydraulic designs are the most lightweight and compact. Unfortunately, most hydraulic dampers exhibit distinctly nonlinear damping characteristics. The nonlinearity arises because these designs employ orifices, through which flow cannot develop fully. Using capillaries, through which flow can develop, provides a linear pressure-flow characteristic. However, unlike an orifice, the size (i.e. diameter) of a capillary is difficult to adjust. Therefore, a damper with several parallel channels, each of which can be valved on or off is designed. By sizing these channels so that their conductances (inverse resistances) are related in a binary fashion, the overall flow conductance can be easily programmed.

2.1 BINARY DAMPER MODELING

In the design shown schematically in Figure 2, each channel is an annulus and is governed by the equation:

$$\Delta P = R_i Q_i \tag{1}$$

where ΔP is the pressure drop from one end of the channel to the other, Q_i is the flow rate through a given channel, and R_i is the fluid resistance of the channel. R_i is purely a function of the geometry of the annulus (inner radius a, outer radius b, length L) and the viscosity of the fluid in the damper (μ). For fully developed flow through an annulus [17]:

$$R_i = \frac{\pi}{8\mu L}\left[\left(b_i^4 - a_i^4\right) - \frac{\left(b_i^2 - a_i^2\right)^2}{\ln\left(\frac{b}{a}\right)}\right]^{-1} \tag{2}$$

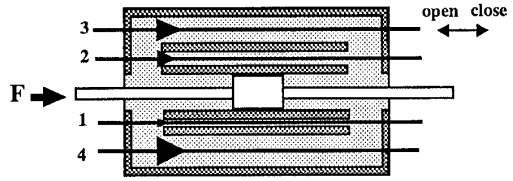

Figure 2: Multi-channel damper with individual channel valves. This damper can be configured for a variety of fluid paths and fluid conductances.

From mass conservation, the total flow, Q_{tot}, is the sum of the flow through all the channels.

$$Q_{tot} = Q_1 + Q_2 + \cdots + Q_n = \Delta P\left[\frac{1}{R_1} + \frac{1}{R_2} + \cdots + \frac{1}{R_n}\right] \tag{3}$$

Because the system is closed and continuous, the velocity and force of the piston can be related to the flow and pressure drop in the fluid. The force on the piston creates the pressure drop across the channels and the piston must travel at the same rate as the fluid. Mathematically, this relationship is:

$$V = \frac{Q_{tot}}{A_p} \tag{4}$$

$$F = \Delta P A_p \tag{5}$$

where A_p is the piston cross-sectional area.

Rearranging equations (4) and (5) and substituting for Q_{tot} and ΔP in equation (3), produces:

$$VA_p = \frac{F}{A_p}\left[\frac{1}{R_1} + \frac{1}{R_2} + \cdots + \frac{1}{R_n}\right] \tag{6}$$

Therefore, the mechanical conductance (inverse damping coefficient), B^{-1}, and the fluid resistance of the individual channels are related by:

$$B^{-1} = \frac{V}{F} = \frac{1}{A_p^2}\sum_{i=1}^{n}\frac{1}{R_i}, \tag{7}$$

where n is the number of channels. By defining the fluid conductance of each channel as $C_i = 1/R_i$, equation (7) becomes:

$$B^{-1} = \frac{1}{A_p^2}\sum_{i=1}^{n} C_i, \tag{8}$$

It should be noted that this summing of conductances is a direct result of the common pressure drop across all channels.

The term "binary" is used to describe this damper because the channels are constructed such that the conductance of each channel diameter is a factor of two larger than that of the next smaller channel:

$$\begin{aligned} C_1 &= C \\ C_2 &= 2C \\ C_3 &= 4C \\ &\vdots \\ C_n &= 2^{(n-1)}C \end{aligned} \tag{9}$$

The preceding model is based on two simplifying assumptions. The first assumption is that the relationship between pressure and flow rate in each channel is *linear*. In order for this to hold true, the entrance effects at each channel and any unsteady effects must be negligible. An empirical relation for the entrance length, where flow is laminar but not fully developed is:

$$L_e = .06dRe, \tag{10}$$

where d is the hydraulic diameter of the annulus and Re is the Reynold's number [17]. For the entrance effects to remain negligible the ratio of the entrance length to the total channel length must be much less than 1 ($Le/L<<1$). For design purposes, a ratio of .1 is acceptable.

The second assumption in this model is that steady flow occurs through all channels. For steady flow, inertia terms disappear and viscous terms dominate. To check that this is indeed the case, the time constant for inertial effects to die out is compared to the expected time constant of the manipulator. The longest time constant will be associated with the largest channel and can be approximated by:

$$\tau = \frac{(b-a)^2}{\nu}. \tag{11}$$

The time constant for steady flow is ~2 ms whereas we expect the fastest time constant for the manipulator to be ~100 ms: therefore, inertial effects can be ignored.

2.2 BINARY DAMPER PROTOTYPE

The actual dimensions of a prototype Binary Damper are shown in Figure 3 . Seven channels plus leakage through the main piston shaft are used to obtain a range of conductances from $1C$ (all channels closed, leakage past main piston only) to $128C$ (all channels open).

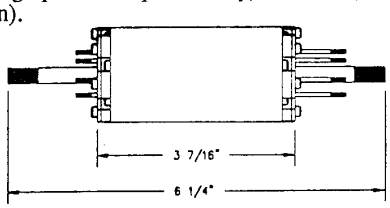

Figure 3: Dimensions of prototype binary damper.

3. TUNEABLE SPRING

The second PPI component is a programmable spring. Designing a spring presents different issues. Unlike the damper which dissipates energy, a spring stores energy. Therefore, it is necessary to account for the energy in the spring at any given time. Many potential programmable spring designs contain *memory*, in other words the energy stored in the spring is a function of its history. Designing a *memoryless* spring avoids the necessity of tracking past states. The initial criterion is, then, that the stiffness of the spring and the current displacement should uniquely define the energy in the spring such that the history of the spring is irrelevant. A related goal is that the equilibrium point, where the energy is minimum, should be at all times well-defined. Other design goals include: stiffness range of at least two orders of magnitude, high bandwidth, linearity, light weight, and compactness.

3.1 ANTAGONISTIC NONLINEAR SPRINGS

With these criteria in mind, there are several options for a programmable spring. A helical spring with varying coil sizes used in compression would change stiffness as the coils bottom out. A simple cantilever beam whose length can be changed to change the stiffness is another option. These methods present some difficulty in terms of packaging. Variable reluctance electromagnetic devices can provide excellent linearity and dynamic range, but are far too heavy and bulky for this application. Pneumatic devices, although reasonably lightweight and compact, are highly nonlinear and are difficult to control due to the significance of thermodynamic effects.

The programmable spring developed here is reminiscient of human muscle operation. The human arm is actuated through antagonistic pairs of muscles acting across the joints. It has been noted that these muscles often behave like tuneable springs, changing the stiffness and equilibrium joint angle of the arm [9].

Similarly, the spring system designed here consists of two nonlinear springs acting in opposition. The basic design concept is shown in Figure 4. Two identical non-backdriveable actuators are connected to the link via identical, nonlinear springs.

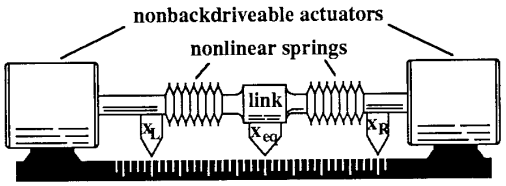

Figure 4: Schematic of a device with programmable stiffness and equilibrium position.

If the springs are manufactured to exhibit the force-displacement relationship of a signed quadratic, i.e. $f = K\text{sign}(x)x^2$, then the stiffness of the link becomes exactly *linear*. Figure 5 shows the force-displacement curves of two such springs. In the middle region,

$$f_1 = K(x-x_L)^2$$
$$f_2 = -K(x-x_R)^2. \quad (12)$$

The system force-displacement curve is the sum:

$$f_1 + f_2 = K(x^2 - 2xx_L + x_L^2 - x^2 + 2xx_R - x_R^2)$$
$$= 2K(x_R - x_L)\left[x - \frac{1}{2}(x_L + x_R)\right] \quad (13)$$

The stiffness is proportional to the difference of x_R and x_L: $K_{link} = 2K(x_R - x_L)$; while the equilibrium position proportional to the sum of x_R and x_L: $x_{eq} = (x_R + x_L)/2$. Thus, by treating $x_R - x_L$ and $x_R + x_L$ as control inputs, stiffness and equilibrium become decoupled.

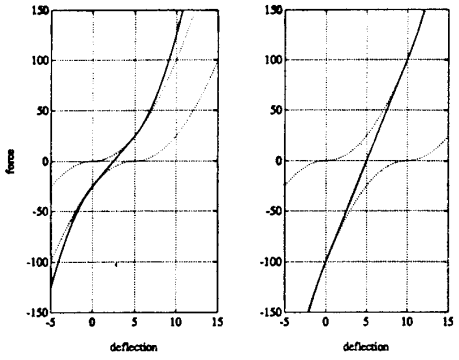

Figure 5: Two examples of the summing of signed quadratic spring characteristics. Individual spring characteristics are shown as dotted lines. In (a) x_L=0 and x_R=5. The sum (solid line) is linear between these points, has an equilibrium point at x_{eq}=2.5, and a slope of K_{link}=10. The same nonlinear springs are shown in (b) but with x_L=0 and x_R=10. The sum is again linear between these locations, but now x_{eq}=5 and the slope is K_{link}=20.

The design challenge becomes one of fabricating a nonlinear spring with similar characteristics. Such springs can be referred to as "hardening" springs: the more they deflect the stiffer they become. Material strength is higher in tension than in bending, and any shape which flattens out as it deflects should provide a hardening characteristic. Springs with carefully chosen geometric nonlinearities (e.g. sine waves or circular arcs) are investigated. Springs shaped like a sine wave or a series of circular arcs are examples. The exact force-displacement curve of a variety of shapes can be studied.

3.2 LUMPED-PARAMETER MODEL

Curved beams subjected to bending have been studied for some specific geometries [4]. However, to study *any* shape that might have the desired force-displacement curve, a computer simulation is used. Due to the complexity and intractability of this problem through analytical methods, a lumped-parameter model is used to analyze various spring shapes. The model is based on the minimum potential energy of a system of rigid links and springs as shown in Figure 6. Symmetry allows study of half of the spring at a time.

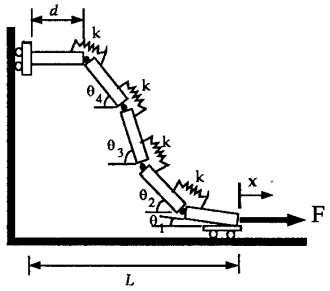

Figure 6: Lumped-parameter model of a nonlinear spring.

The potential energy of the model is:

$$U = \frac{1}{2}\sum_{i=1}^{n} k_{i,i+1}\left[(\theta_{i+1} - \theta_i) - (\theta_{i+1} - \theta_i)_o\right]^2 + \lambda\left[\sum_{i=1}^{n}(d\cos\theta_i) - L\right] \quad (14)$$

with n being the number of rigid links in the model. The LaGrangian multiplier, λ, represents the force on the spring . This constraint is identically zero and does not affect the system's energy.

When the potential energy of the system is minimum, its partial derivative with respect to each of the degrees of freedom equals zero. The result is a system of nonlinear simultaneous equations:

$$\frac{\partial U}{\partial \theta_i} = k_{i,i+1}\left[(\theta_{i+1} - \theta_i) - (\theta_{i+1} - \theta_i)_o\right] - k_{i-1,i}\left[(\theta_i - \theta_{i-1}) - (\theta_i - \theta_{i-1})_o\right]$$
$$+ \lambda\left[(d\sin\theta_i)\right] = 0$$

$$\frac{\partial U}{\partial \lambda} = \left[\sum_{i=1}^{n}(d\cos\theta_i) - L\right] = 0 \quad (15)$$

To generate the force-displacement curve for a given spring shape, a series of displacements are imposed on the model and the resulting forces are recorded.

The error in the lumped-parameter model can be determined by comparing the analytical and lumped-parameter solutions of a similar but simpler case -- the cantilever beam. Figure 7 shows the cantilever beam in an analytical case and in the lumped-parameter model. The Euler equation for deflection of a beam loaded as shown is:

$$\delta = \frac{1}{3}\frac{PL^3}{EI} \quad (16)$$

whereas the lumped-parameter solution is

$$\delta = \left[\frac{(n+1)(2n+1)}{6n^2}\right]\frac{PL^3}{EI} \quad (17)$$

As the number of links in the model increases, the error approaches zero, or equivalently:

$$\text{as } \left[\frac{(n+1)(2n+1)}{6n^2}\right] \rightarrow \frac{1}{3}, \quad \text{error} \rightarrow 0 \tag{18}$$

For the case of n=15, the error is approximately 10%.

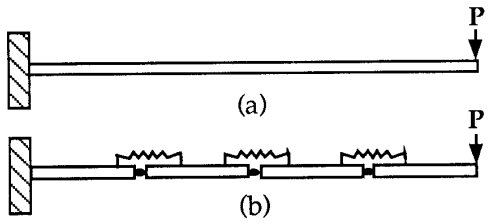

Figure 7: Cantilever beam: (a) continuous, analytical model (b) lumped-parameter model

3.3 EQUILIBRIUM POSITION, STIFFNESS AND MOTION

As previously mentioned, the equilibrium position must be readily determined for the two-spring system. The springs being identical, the equilibrium position is always half way between them. The endpoint locations, x_L and x_R, of each spring set the equilibrium position uniquely at $(x_R + x_L)/2$, even if the springs are not quadratic. The system stiffness is functionally dependent on, but not linearly related to, x_R-x_L. A pair of motors is used for setting stiffness and moving the link. By turning the motors in opposite directions at the same speed, the stiffness is changed but the link does not move. Turning the motors in the same direction at the same speed, the stiffness remains constant but the link moves. Finally, turning the motors at different speeds in the same direction, the stiffness hanges *and* motion occurs.

3.4 TUNEABLE SPRING PROTOTYPE

The dimensions of the spring prototype are given in Figure 8. The configuration shown is of two springs fastened together for better stability. The ease of making a circular arc was a major consideration in this design, as well as the force-displacement curve. A die was designed and made to press these springs out of spring steel stock. For purposes of concatenation, the zero slope at the point of force application is desirable.

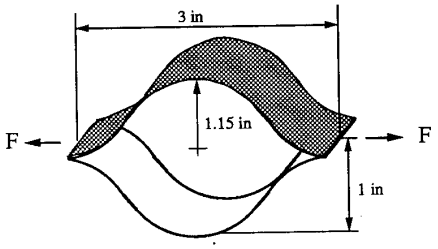

Figure 8: Spring prototype dimensions.

A comparison of the theoretical and actual force-displacement curves is illustrated in Figure 9. The long, almost linear range at low stiffness is beneficial because at low stiffness, larger displacements are expected and this provides a constant, linear stiffness during the entire deflection. Eighteen links were used in the lumped-parameter model with approximately 8% error. The dynamic range of single prototype is approximately 60. Several of these springs can be combined in series or parallel to provide the desired system behavior.

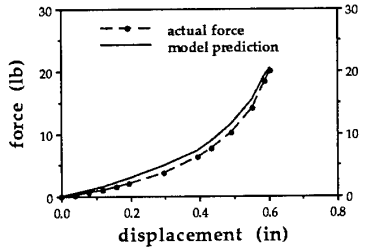

Figure 9: Plot of both the theoretical and actual force-displacement curves for the nonlinear spring prototype.

In order to see the entire spring system characteristics, the force-displacement curves of the two springs in opposition are added for various equilibrium points (stiffness settings). Figure 10 shows a range of force-displacement curves for the prototype spring system. Note that some linear or nearly linear range exists for all equilibrium positions. At higher levels of stiffness, the linear range is smaller, but any deflection from equilibrium should also be smaller.

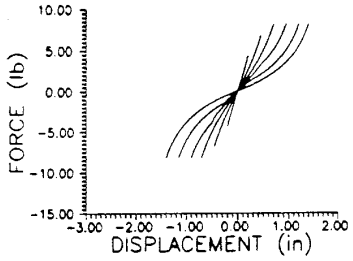

Figure 10: Force-displacement curves of thespring system prototype for various equilibrium positions.

4. SYSTEM PERFORMANCE

The PPI components developed in the preceding sections will be used in a single link manipulator (SLM) to examine basic operational and control issues, and to provide preliminary indication of system level performance. The design of that manipulator and its expected behavior are described here.

The characteristic equation of motion of the manipulator in Figure 11 is:

$$J\ddot{\theta} + Br_1^2\dot{\theta} + Kr_2^2\theta = Kr_2x_c. \tag{19}$$

where J is the moment of inertia, B is the damping coefficient, K is the stiffness coefficient, r_1 is the radius of the

pulley connected to the damper, r_2 is the radius of the pulley actuated by the spring system and x_c is the control input.

The manipulator natural frequency, ω_n, and damping ratio, ζ, are:

$$\omega_n = \sqrt{\frac{Kr_2^2}{J}} \tag{20}$$

$$\zeta = \frac{Br_1^2}{2r_2\sqrt{KJ}} \tag{21}$$

Because K and B can be programmed in real time, ω_n and ζ can be as well. For the spring and damper prototypes described and specific values of J, r_1 and r_2, the natural frequency and the damping ratio of the SLM can be varied across one order of magnitude.

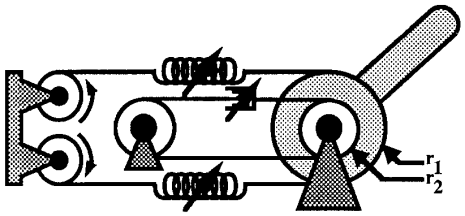

Figure 11: A single-link manipulator utilizing the PPI components: binary damper and nonlinear spring.

5. FUTURE WORK

While it has been demonstrated that PPI components implement impedance control for robust manipulation, substantial work remains. After completing tests and adjustments of the prototypes, the single link manipulator will be constructed. This manipulator will serve as a valuable research tool in many areas: formulation of interactive task specifications, further investigation of impedance control via passive elements, and much more. The intention is to incorporate these PPI components into a multiple link manipulator as well. Such a manipulator will be able to accomplish a greater variety and complexity of tasks. In addition, investigations of how actuator and kinematic redundancies, in combination with PPI components, can be used to simplify the planning and execution of high-speed assemblies must be made. The development of working PPI components opens the door to all kinds of interesting areas of research.

REFERENCES

[1] An, C.H. and Hollerbach, J.M. "Dynamic stability issues in force control of manipulators." *Proceedings of the IEEE International Conference on Robotics and Automation*, pp. 890-896. IEEE Press (1987).

[2] Colgate, E. and N. Hogan. "An analysis of contact instability in terms of passive physical equivalents." *Proceedings of the 1989 IEEE International Conference on Robotics and Automation*. IEEE Press (1989).

[3] Colgate, E. "On the inherent limitations of force feedback compliance controllers." *Robotics Research*, Youcef-Toumi, K., and Kazerooni, H., editors. ASME, New York, December (1989).

[4] Cook, R. and W.C. Young. *Advanced Mechanics of Materials*. MacMillan Publishing.

[5] Cutkosky, M.R. and P.K. Wright. "Active Control of a Compliant Wrist in Manufacturing Tasks." *Journal of Engineering for Industry*; Transactions of the ASME **108**(February): 36-43 (1986).

[6] Eppinger, S.D. and W.P. Seering. "On dynamic models of robot force control." *Proceedings of the IEEE International Conference on Robotics and Automation*, pp. 29-34, 1986.

[7] Goswami, A., M.A. Peshkin, and J.E. Colgate. "Passive Robotics: An Exploration of Mechanical Computation." *Proceedings of the 1990 IEEE International Conference on Robotics and Automation*. IEEE Press (1990).

[8] Hogan, N. "On the stability of manipulators performing contact tasks." *IEEE Journal of Robotics and Automation*, 1988.

[9] Hogan, N. "Tuning muscle stiffness can simplify control of natural movement." *1980 Advances in Bioengineering*, Van C. Mow, editor, ASME, New York, 1980.

[10] Immega, Guy B. "Romac Actuators for Micro Robots." *1987 IEEE Micro robots and Teleoperators Workshop*. IEEE Press (1987).

[11] Kazerooni, H. "Robust, non-linear impedance control for robot manipulators." *Proceedings of the IEEE International Conference on Robotics and Automation*, pp. 741-750. IEEE Press (1987).

[12] Mason, M.T. "Compliance and force control for computer controlled manipulators." *IEEE Transactions on Systems, Man, and Cybernetics*, SMC-11(6): 418-432, June 1981.

[13] Mills, J.K. "Hybrid Actuator for Robot Manipulators: Design, Control, and Performance." *Proceedings of the IEEE International Conference on Robotics and Automation*. IEEE (1990).

[14] Nevins, J.L. and D.E. Whitney. "The force vector assembler concept." *First International Conference on Robotics and Manipulators*, Udine, Italy, September 1973.

[15] Peshkin, M.A. "Programmed Compliance for Error Corrective Assembly." *IEEE Transactions on Robotics and Automation*, Vol. 6, August (1990).

[16] Schimmels, J.M. and M.A. Peshkin. "Force-Assemblability: Insertion of a Workpiece into a Fixture guided by Contact Forces Alone." *1991 IEEE International Conference on Robotics and Automation*.

[17] White, F.M. "Fluid Mechanics." McGraw-Hill, New York (1979).

[18] Whitney, D.E. "Force feedback control of Manipulator Fine Motions." *Proceedings of the Joint Automatic Control Conference*, 1976.

[19] Whitney, D.E. "Historical perspective and state of the art in robot force control." *Proceedings of the IEEE International Conference on Robotics and Automation*, pp. 262-268, 1985.